

# High accurate metrology on large surface areas with low reflectivity

Bastian L. Lindl<sup>1,\*</sup> and Frank Kemnitzer<sup>1</sup>

<sup>1</sup> cyberTECHNOLOGIES GmbH, Bei der Hollerstaude 19, 85049 Ingolstadt, Germany

\* Corresponding Author / E-mail: bastian.lindl@cybertechnologies.com, TEL: +49-841-885330, FAX: +49-841-8853310

KEYWORDS : 3D surface metrology, flatness measurement, chromatic confocal sensor, surface roughness

*Typically 3D interferometers are used to measure large surface areas with nanometer accuracy. The working principle of the interferometer implies a smooth and reflective surface. It is ideally suited for optics, wafers and mechanical parts with low topography and low surface roughness. Measurement is typically the last process step after the surface finish. In many cases the process efficiency and quality can be improved if a surface area is measured at an earlier stage in the process. However, in a non-finished surface condition the interferometer does not fulfill this requirement. To overcome this drawback a different measurement approach is chosen. Confocal white light sensors based on the principle of chromatic aberration combine high dynamic range and excellent signal/noise ratio on various strongly reflecting, rough and steep surfaces. The sensors are available with a z-resolution down to 3 nm. On a precise positioning system this sensor technology scans large areas up to 600 mm with a non-repeatable error of 100 nm. Three key factors enable this level of accuracy: the mechanical system, the calibration and the environmental conditions. The mechanical system is based on a massive granite base with vibration isolation elements. Using the polished granite as a bearing surface, vacuum preloaded air bearings provide maximum accuracy in x, y and z-direction. The sensor head is mounted on a motorized z-axis with a calibrated encoder and 1 nm resolution. To overcome the relatively small measurement range of the high-resolution sensor head, the measurement system offers a function called continuous autofocus. The motion controller and the sensor controller are working in a closed loop mode and the z-axis automatically follows the shape of the part during the scanning process. This extends the height measurement range and effectively the measurement range of the system up to the travel limit of the z-axis. The calibration routines compensate the repeatable error of the motion system and the linearity error of the white light sensor. Stable environmental conditions in a clean room are mandatory. Even the standard compressed air supply is sufficient for the stage to provide submicron accuracy. However, studies have shown that minor variations in air pressure and air temperature are directly impacting the accuracy. Unlike compressed air, nitrogen offers stable pressure and temperature.*

## NOMENCLATURE

$N_a$	= Numerical aperture
$\alpha$	= Angle between optical axis and reflected beam
$\lambda$	= Wavelength

## 1. Introduction

Typically 3D white light interferometers are used to measure large surface areas with nanometer or even sub nanometer accuracy. The working principle of an interferometer is based on the superposition of two waves where the resulting interference pattern is used to calculate some meaningful properties of the measured surface. Especially when using the phase shifting interferometry (PSI) a smooth and reflective

surface is required. Also the vertical scanning interferometry (VSI) implies a sufficient low surface gradient compared to the acceptance angle of the objective<sup>1</sup>. White light interferometry is ideally suited for optics, wafers and mechanical parts with low contours, low surface gradients and low surface roughness. Therefore interferometric measurements are typically the last process step after the surface finish. But in many cases the process efficiency and product quality can be improved, if the surface area is measured at an earlier stage in the production process. However, these pre-finished surfaces often do not fall within the ideal boundary conditions for interferometers. To overcome this drawback we propose a different surface measurement approach.

In this work we present a non-contact surface measurement system based on a chromatic confocal white light sensor in combination with a high precision  $x, y, z$  motion system. Compared to a white light interferometer the implemented sensor is a point sensor, meaning it does not return a two dimensional array of height data points per single

measurement, but rather a single data point. By moving the sample below the sensor, the surface can be rasterized and a complete height data map can be collected. The lateral resolution of such a system depends on the accuracy of the motion system on the one hand, on the other hand the spot size of the point sensor is the second limiting factor. In our system we are typically using a sensor with a spot size of 4  $\mu\text{m}$ . Taking into account the full width at half maximum for the sensor, one will end up with an effective spot size of 2  $\mu\text{m}$ . The positioning accuracy and the linearity of the 350 mm  $\times$  350 mm  $x, y$  motion system is calibrated to be better than 1  $\mu\text{m}$ . The vertical resolution of the sensor is specified with 20 nm for the measurement range of 600  $\mu\text{m}$ . To overcome the limitation of the sensor's small measuring range, we implemented a high precision  $z$ -axis with a vertical resolution down to 1 nm and a travel range of 300 mm. Laboratory measurement have shown a non-repeatable error of 22 nm over the entire measurement volume.

## 2. System design and function

### 2.1 Chromatic Confocal Sensor Principle

Confocal white light sensors, based on the principle of chromatic aberration, combine high dynamic range and excellent signal/noise ratio on various highly reflecting, rough and steep surfaces. The method takes advantage of an optical phenomena, known as chromatic aberration. The axial position of the focal point of an uncorrected lens depends on the color or wavelength of the light that is focused on the surface. In the visible spectral region, the focal distance for blue light is small and increases with the wavelength towards red light. The focal points of other colors are located in between, according to the row: red, orange, yellow, green, blue, violet. Depending on the distance of the target from the focusing lens, light of a very small wavelength region  $\lambda_1$  is focused on the target's surface (Fig 1). All other spectral components of the light source are illuminating a much wider area of the sur-

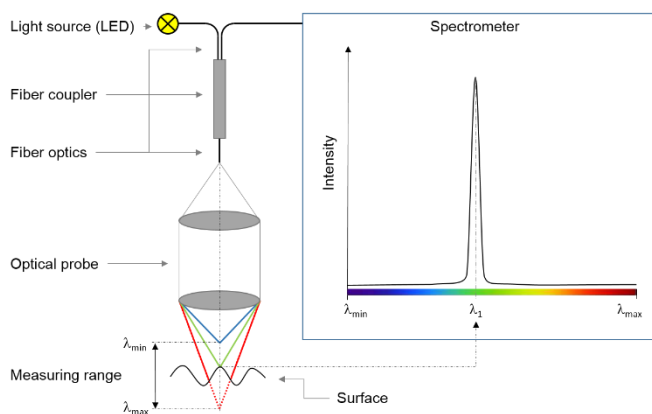


Fig 1: Principle of the chromatic confocal measurement

face. As a consequence, the light going through the fiber to the spectrometer is almost monochromatic with wavelength  $\lambda_1$ , being a unique value for the distance between optical probe and the sample surface.

The sensor consists of a control unit, a fiber connection and a measurement head. The control unit contains a white light source and a spectrometer. Its light is transmitted to the measurement head using a multimode fiber. The measurement head, also referred to as "sensor", focuses the light onto the object to be measured and couples the reflected light back into the fiber. This reflected light returns to the spectrometer

inside the control unit, where the spectral composition of the intensity is measured by a line detector. Using optical heads with a high numeric aperture allows for measuring polished, rough, highly reflective or opaque surfaces, at a slope of up to 45  $^\circ$  to the probe's optical axis (limited by the numerical aperture  $N_a = \sin(\alpha)$ ). Selecting only the perfectly focused part of the reflected light, the effective measurement spot size is very small, yielding a lateral resolution of up to 2  $\mu\text{m}$ . Different from many others, the above described optical measuring principle tolerates shadowing effects, caused by edges or holes with high aspect ratio. Furthermore it reduces the unavoidable measurement errors of triangulating and confocal measurement principles, which are caused by speckle effects and represent a strong physical limitation to measuring accuracy, by taking advantage of a short coherent light source and high numerical observation aperture. The accuracy of the distance measurement also depends on the scattering properties of the target surface. Highly absorbing materials and rough or tilted surfaces reduce the amount of reflected light, entering the optical probe, hence reducing the signal to noise ratio significantly. This is compensated by increasing the exposure time and/or by the use of extremely bright illumination sources. The measurement sensors are available in various forms with a  $z$ -resolution down to 3 nm, different measurement ranges and numeric apertures<sup>2</sup>.

### 2.2 Motion system

Due to the fact that the sensor described in the previous section is a point sensor, there are great demands put on the  $x, y, z$  motion system. The surface of the measurement object is built by taking separate point measurements at different stage positions. Therefore the maximum possible surface size is limited by the travel length of the  $x$  and  $y$  axis. Available travel lengths go up to 600 mm  $\times$  600 mm. The minimum lateral distance between two data points is limited by the spot size of the sensor to 1  $\mu\text{m}$ . This results in a theoretical surface consisting of 36 billion data points. Understandably, the overall measurement accuracy is directly correlated to the axes accuracy. In fact, if the  $x, y$  stage has a certain non-repeatable error (all other errors can be calibrated out), this non-repeatability will have a direct impact on the overall system accuracy. The particular system presented in this paper has a  $x, y$  travel of 350 mm  $\times$  350 mm. To minimize the non-repeatable errors we decided to use a custom air bearing setup. The stage itself is manufactured as

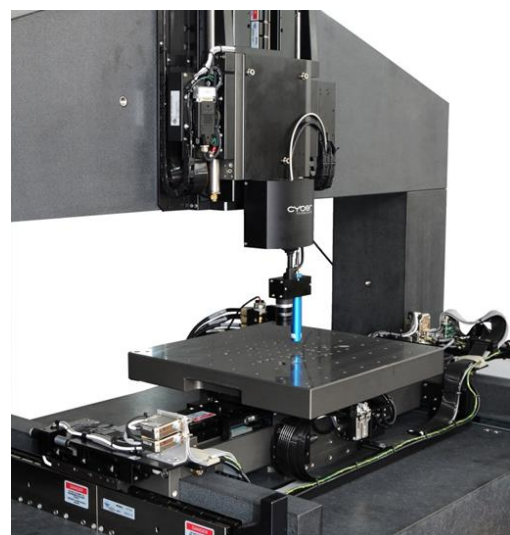


Fig 2: CT350S system overview

one big air bearing, which uses the polished granite base as a bearing surface in combination with a vacuum preload. The driving force behind the stage are brushless linear servomotors with ironless forces, which means there is zero cogging and no attractive forces, resulting in very smooth motion. To accomplish this, we use a design with two  $y$ -axes and one  $x$ -axis as seen in figure 2. The two axes are also designed with air bearings, both again using polished granite surfaces as the base of the bearing. The sensor head is mounted on a motorized  $z$ -axis, also using a linear drive with air bearings. To compensate for the gravitational force, a pneumatic counter balance was introduced, allowing for a very stable and smooth vertical motion. The machine is equipped with 4 membrane air-spring isolators to not only provide level control on the machine, but also provide mechanical isolation between the machine and the environment. Each isolator has an adjustable needle valve between the damping cavity and the load chamber that can be used to individually tune each isolator for the required damping. In addition, the systems base is equipped with 8 adjustable velocity controlling dampers mounted horizontally to minimize the motion of the base during operation. Nevertheless we still recommend placing the machine on a stable grounding. In our tests, the system was placed on a special grounding, being isolated against the rest of the building's basement.

### 2.3 Large scale measurements

The sensor head installed on the machine we are presenting in this paper, has a measurement range of 600  $\mu\text{m}$  with a resolution of 20 nm. The encoder outputs from all three axes are directly connected to the sensor controller, ensuring a unique association to each sensor value. The sensor runs at a maximum sampling rate of 4 kHz, meaning it is collecting 4000 individual height data points per second. Depending on the current stage position and the user's scan definition, the software automatically decides if the measured data point (and the latched axes positions) should be saved or not. This way, we can do on-the-fly measurements - the stage does not need to stop at each data point position.

Start	25.000 mm	50.000 mm	<input type="button" value="↕"/>
End	275.000 mm	300.000 mm	<input type="button" value="↕"/>
Travel	250.000 mm	250.000 mm	<input type="button" value="↔"/>
Step	0.010 mm	0.010 mm	<input type="button" value="↔"/>
Shape	Rectangular		
Axis	Automatic <input checked="" type="checkbox"/> Bidirectional		

Fig 3: Typical setup for a rectangular raster scan

In fact, assuming bidirectional scanning is enabled, the stage performs a motion along a meandering pattern for a typical rectangular raster scan. This approach allows us to minimize the scanning time and reduce the impact of environmental influences like temperature or air pressure as much as possible. Figure 3 shows a typical setup for a large scale rectangular raster scan. The necessary parameters are the stage's start and end position, the travel length in  $x$ - and  $y$ -direction and the step size in  $x$ - and  $y$ -direction, meaning the distance between two adjacent data points. Besides rectangular rasters the system is able to perform circular or annular raster measurements to save time. Especially for ring-shaped samples this mode can save up to 90 % of scanning time.

### 2.4 Extending the sensor's measurement range

As described previously, the measurement range of the selected sensor is 600  $\mu\text{m}$ . Depending on the height of the sample this range might be a limiting factor for the respective measurements, requiring

```

1 WHILE TRUE
2   sensorValue = READANALOGINPUT()
3   IF sensorValue IS VALID
4     axisPosition = READAXISPOSITION()
5     averageValue = FLOATING_AVERAGE(sensorValue + axisPosition)
6
7     IF ABS(averageValue - axisPosition) > threshold
8       MOVE(Z, averageValue)
9     END IF
10  END IF
11 END WHILE

```

Fig 4: Motion controller firmware pseudo code for continuous  $z$ -axis auto tracking to keep sensor in range

repeatable scans of the same area at different height levels and stitching of the resulting rasters at the conclusion of the scan. A superior solution for this use case was implemented in the described system. A programmed control loop, running on the firmware of the motion controller in real-time, always ensures that the sensor is in focus. To accomplish this, the analog output of the sensor is directly connected to an input of the motion controller. The firmware program on the motion controller is continuously evaluating the received sensor height value and auto tracking the  $z$ -axis to keep the sensor within its measurement range. As seen in figure 4, the firmware program implements a hysteresis by only sending a new move command to the axis, when the difference between the required position and the actual position is greater than a certain threshold. This ensures that the axis is not introducing any vibration due to the sensor noise. To further reduce the risk of an uncontrolled correctional move, a floating average is calculated over the last few sensor values received. This will filter out false readings or outliers up to a certain degree. The drawback of this method is, that the surface has to be sufficiently smooth, meaning there are no steps allowed that are greater than the sensor range. In fact, as the auto tracking function keeps the sensor in the middle of its range most of the time, the maximum allowed discontinuous step height would be  $\pm 300 \mu\text{m}$ . The measurement will be aborted automatically if the sensor is out of range for a configurable amount of time, preventing the sensor head from crashing into the sample. As mentioned in the previous section, all axis position (including the  $z$ -axis positions) are latched to the sensor value. To return an extended height value, the current  $z$ -axis position is added to the actual sensor reading. As we are still measuring on-the-fly (the stage is moving during the measurement) this method introduces some artifacts arising from the fact that the  $z$ -axis is moving during the integration time (0.25 ms for a 4 kHz sampling rate) of the sensor. To compensate for these artefacts we assume a linear motion for the  $z$ -axis and therefore we can calculate an interpolated  $z$ -axis value, taking the previous  $z$ -axis position and the actual  $z$ -axis position. In that way we have extended the measurement range of our system from 600  $\mu\text{m}$  to over 300 mm. Experiments have shown that the accuracy of the combined height value can be even better than height data taken only from the sensor. The reason for this is because the signal to noise ratio for the sensor is best in the middle of its range and because the accuracy of the sensor decreases on steep slopes, due to the lower intensity of the reflected light.

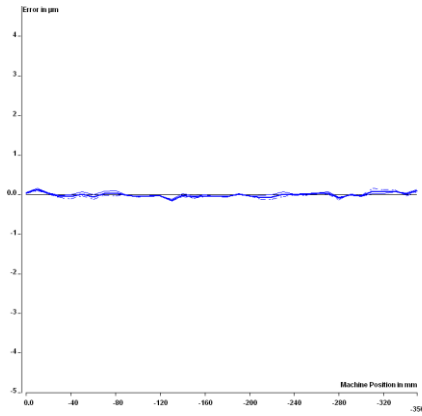


Fig 5a Linear error plot of x axis.

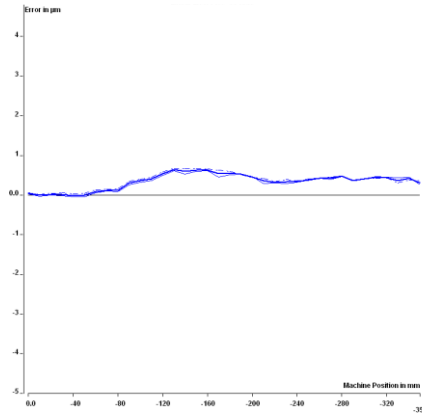


Fig 5b Linear error plot of y/y axis

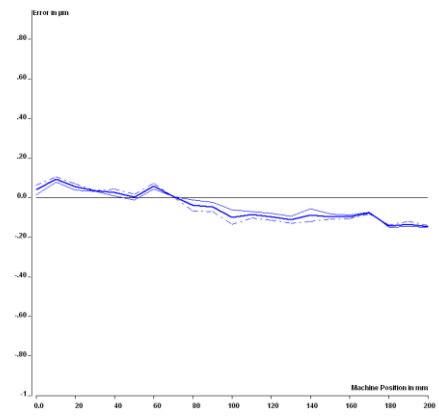


Fig 5c Linear error plot of z axis

### 3. Results

To verify the performance of the system we started to test the linearity and (bidirectional) repeatability of the calibrated axes. Figure 5 shows the results for all available axes in the system. The bidirectional repeatability was determined to  $\pm 0.064 \mu\text{m}$  for  $x$ ,  $\pm 0.085 \mu\text{m}$  for  $y$  and  $\pm 0.037 \mu\text{m}$  for  $z$ . The calibrated axis accuracy is  $\pm 0.158 \mu\text{m}$  for  $x$ ,  $\pm 0.365 \mu\text{m}$  for  $y$  and  $\pm 0.133 \mu\text{m}$  for  $z$  over the entire range of travel. The alignment between  $x$  and  $y$  was measured to 1.18 arc sec, the alignment of  $z$  to the  $xy$  plane is 13.75 arc sec. These numbers look very promising but actually do not tell a lot about the performance of the system for an actual scan. Due to the fact that a usual measurement can take form several minutes up to several hours, depending on the used lateral resolution (stepsize) and sampling rate of the sensor, we first need to minimize the environmental influences to the system. To get an idea of the influence of pressure or vacuum fluctuations we varied the supply pressure to the system and recorded the output of the displacement sensor. As seen in figure 6 the displacement between the optical flat (resting on  $x$  carriage) and the displacement sensor (mounted on the  $z$  carriage) changed linearly with respect to supply pressure at the rate of  $12.64 \mu\text{m}/\text{MPa}$ . Fluctuations of vacuum supply pressure have a similar effect with a rate of  $91.5 \mu\text{m}/\text{MPa}$ . The effect of temperature changes is approximated by looking at the coefficient of expansion for the different materials. The  $x$  carriage and the mounting plate are aluminum with a coefficient of  $23.6 \text{ ppm}/\text{K}$  (size 170 mm), the granite structure has  $3.9 \text{ ppm}/\text{K}$  (753 mm to the middle of the  $z$  axis). For temperature changes of the entire system as a whole, the  $x$  carriage and the granite bridge expansions partially cancel each other. The thermal ex-

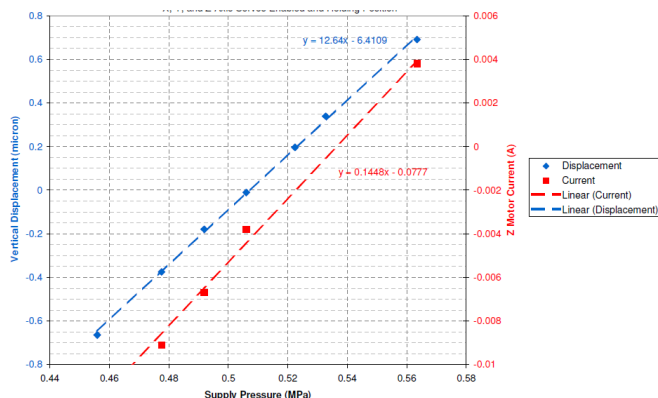
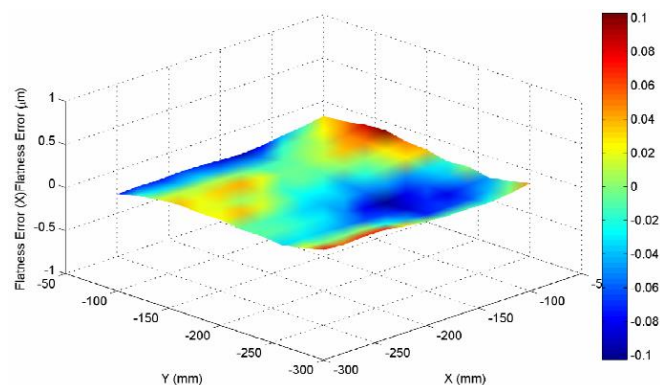


Fig 6 Vertical displacement and z motor current vs. supply pressure

pansion of the bracket that mounts the height sensor to the  $z$  stage dominates the relative gap change. For a bracket holding made of aluminum this results in  $11 \mu\text{m}/\text{K}$ , for a bracket holding made of INVAR this yields to  $1.5 \mu\text{m}/\text{K}$ . Even as the INVAR value is much better than the expansion for aluminum we still have to ensure that the temperature variation during the measurement are as low as possible as they will have a direct impact on the height values. Temperature variations on the air supply will also affect the measurement: The  $x$  carriage height variation versus carriage temperature ratio is  $4.0 \mu\text{m}/\text{K}$ . The interface bracket mounted to the  $z$  carriage will also be influenced by the air supply temperature. Depending on the material chosen, the effect on the relative displacement could also be significant. Therefore, for the following tests, the system is located in a cleanroom, with temperature variation  $< 0.1^\circ \text{C}$  during the measurements (recorded by temperature sensors around the system). To reduce the effect of pressure fluctuations and air supply temperature variations, the air supply for the air bearings and  $z$  counterbalance is taken from a dedicated nitrogen tank in combination with a 26.5 liter accumulator tank to further dampen potential fluctuations in air supply pressure. A dedicated vacuum pump for the air bearing preload is used. We used an optical flat with dimensions of  $300 \text{ mm} \times 300 \text{ mm}$  for these tests. As briefly discussed in the sections before, the most important value for us to determine the performance of the system is the non-repeatable error which is measured by the sensor. The optical flat ( $300 \text{ mm} \times 300 \text{ mm}$ ) was placed on the stage and the surface was repeatedly scanned. The result of one of these measurements is shown in figure 7 and represents the actual flatness error of the system, determined to be  $0.205 \mu\text{m}$ . The main reasons for this error are the cumulated errors described earlier and seen in figures

Fig 7 Uncompensated flatness error of the system ( $0.205 \mu\text{m}$ )

5a - 5c. This error can be further reduced by calibrating the system using the same optical flat as was used before. The optical flat is rasterized with 3.0 mm by 3.0 mm step size in  $x$  and  $y$  direction and saved as a machine parameter. Each measured sensor value is then corrected

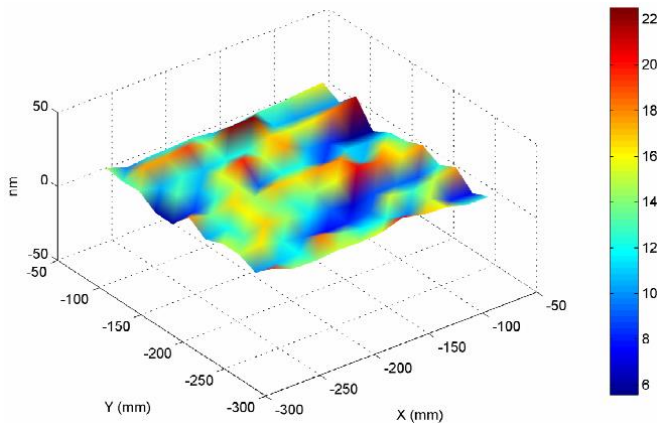


Fig 8 Compensated flatness error on a calibrated system ( $0.022 \mu\text{m}$ )

with the flatness error value at the current  $x, y$  axis position using bicubic interpolation. The resulting error will be the non-repeatable part of the flatness error. Figure 8 shows the result for a measurement on the optical flat after the flatness calibration. The remaining peak to peak error is  $0.022 \mu\text{m}$ , meaning that the system is able to measure large scale surfaces (proved for a  $300 \times 300 \text{ mm}^2$  flat) with an overall accuracy in  $z$ -direction of 22 nm.

### 3. Conclusions

The combination of a high accuracy  $z$ -axis and a high resolution sensor head in addition to an algorithm for real-time auto tracking has resulted in a new and more powerful method of measuring large scale surfaces. We successfully designed a system with a  $x, y$  stage using custom air bearings and mounted a 300 mm  $z$ -axis on a granite bridge above the stage, resulting in a measurement volume of  $350 \times 350 \times 300 \text{ mm}^3$ . The overall system accuracy in  $z$ -direction was determined to be 22 nm for objects with dimensions up to  $300 \times 300 \text{ mm}^2$ . With the auto tracking feature the measurement range had been extended to the entire travel of the  $z$ -axis.

The system was designed for a wide range of applications, beginning with the measurement of large aspherical lenses. Usually large lenses are measured using several interferometer scans, combined in the final step by a sophisticated stitching routine. A problem arises for lenses with steep aspheric slopes, where common interferometers will fail. Our technology provides an easy and very accurate way to measure this kind of optics. Another large field of applications are high accurate flatness measurements, necessary for example to measure the flatness of high performance mechanical seals used in jet engines. In addition, if more than one measurement sample (e. g. for ceramic substrates) fit on the  $x, y$  stage, the system can be programmed to measure part by part using a simple step-and-repeat pattern. This saves a great amount of time and simplifies the measurement process, especially for tasks where many samples of the same type need to be measured. Future development will mainly be focused on the integration of new sensor types to the system, in particular confocal microscopes or confocal laser scanners. This will further increase the range of applications, considering the possibility to combine two or more different sensor types for the same measurements: For example, take a large scale scan with the chromatic sensor and automatically refine specific regions of interest with the measurement of a confocal microscope.

1. Gao, F., Leach, R. K., Petzing and Coupland, J., "Surface measurement errors using commercial scanning white light interferometers," *Meas. Sci. Technol.*, Vol. 19, No. 1, 2008.
2. Michelt, B. and Schulze, J., "The spectral colours of nanometers," *journal Mikroproduktion*, No. 3, 2005.